Environmental Pollution 243 (2018) 582–590

Contents lists available at ScienceDirect

Environmental Pollution

journal homepage: www.elsevier.com/locate/envpol

# Radiological comparison of a FDNPP waste storage site during and after construction☆

D.T. Connor [a, *], P.G. Martin [a], H. Pullin [a], K.R. Hallam [a], O.D. Payton [a], Y. Yamashiki [b], N.T. Smith [c, d, e], T.B. Scott [a]

[a] Interface Analysis Centre, HH Wills Physics Laboratory, University of Bristol, Bristol, BS8 1TL, UK
[b] Graduate School of Advanced Integrated Studies in Human Survivability (GSAIS), Kyoto University, Kyoto, 606-8501, Japan
[c] National Nuclear Laboratory, 5th Floor, Chadwick House, Birchwood Park, Warrington, WA3 6AE, UK
[d] Schools of Earth and Environmental Sciences, University of Manchester, Manchester, M13 9PL, UK
[e] Mechanical, Aerospace and Civil Engineering, University of Manchester, Manchester, M13 9PL, UK

ARTICLE INFO

*Article history:*
Received 10 April 2018
Received in revised form
28 July 2018
Accepted 31 August 2018
Available online 5 September 2018

*Keywords:*
Fukushima
Gamma-spectrometry
UAV
Remediation
Photogrammetry

ABSTRACT

The clean-up effort that is occurring across the region affected by the 2011 Fukushima Daiichi Nuclear Power Plant accident is unprecedented in its magnitude as well as the financial cost that will eventually result. A major component of this remediation is the stripping of large volumes of material from the land surface, depositing this into large waste storage bags before placing these 1 cubic meter bags into specially constructed stores across Fukushima Prefecture.

In this work, using an unmanned aerial vehicle to perform radiological surveys of a site, the time-resolved distribution of contamination during the construction of one of these waste storage sites was assessed. The results indicated that radioactive material was progressively leaching from the store into the surrounding environment. A subsequent survey of the site conducted eight months later revealed that in response to this survey and remedial actions, the contamination issue once existing on this site had been successfully resolved. Such results highlight the potential of low-altitude unmanned aerial systems to easily and rapidly assess site-wide changes over time – providing highly-visual results; therefore, permitting for prompt remedial actions to be undertaken as required.

Use of UAV radiation mapping and airborne photogrammetry to produce a time-resolved assessment of remediation efforts within a Fukushima temporary storage facility.



## 1. Introduction

In March 2011, the INES Level 7 accident at the Fukushima Daiichi Nuclear Power Plant (FDNPP) released a considerable quantity of radiological contamination into the environment – with the impacts felt globally as well as locally. As a direct result of the incident, nearly 150,000 people were evacuated from their homes under the direction of the government, with many of the towns and villages located within Fukushima Prefecture still, to this date, abandoned (Kurokawa et al., 2012). The area affected by the radiation, which is hundreds of square kilometres in size, was subsequently divided into various geographical regions dependent on the level of contamination (quantified by the detected dose-rate) observed during multiple survey works (METI, 2015, 2011). These sub-areas are defined as: areas that are most heavily radiologically contaminated, into which residents will have difficultly returning for the foreseeable future ('Area 3'); areas into which residents are not permitted to live ('Area 2'); and those areas within which remediation works have been conducted or only moderately contaminated and therefore evacuation orders are ready to be lifted ('Area 1'). At present, the original spatial extent of some of these zones have been relaxed or downgraded as the fallout material has decayed through time and remediation operations have been successful. A more recent detailing of these extent of these zones can be found within (METI, 2017).

Some of the primary isotopes released, and therefore the subject of extensive study and remedial action are radioisotopes of Cs ($^{134}$Cs and $^{137}$Cs). Various studies have estimated the total activity of both isotopes from the FDNPP accident to be between 15 and 20

☆ This paper has been recommended for acceptance by Dr. Hageman Kimberly Jill.
* Corresponding author.
*E-mail address:* dean.connor@bristol.ac.uk (D.T. Connor).

https://doi.org/10.1016/j.envpol.2018.08.099

PBq (Aoyama et al., 2016; Buesseler et al., 2017) – considerably less than that emitted into the environment following the Chernobyl accident 25 years earlier (Steinhauser et al., 2014). Following this earlier release, countless studies have been performed examining the behaviour of Cs within the physical environment. Such works have found that the species has a strong affinity for sorption onto the highly-reactive edge-sites of mica and clay-type minerals – where they are difficult to remove/become desorbed, even in harsh chemical situations not observed in nature (Comans & Hockley, 1992; Cremers, Elsen, Preter, & Maes, 1988; Sawhiney, 1972). Due to this, Cs is transported bound to particulate material, rather than as ionic species within solution.

As part of this remediation work, which has occurred extensively within Area 1 over the past 6 years since the accident, a vast volume of contaminant material waste has been produced. Similar remediation work, albeit on a smaller scale, has also been ongoing outside the restricted zones. This has resulted in the construction of temporary storage facilities, similar in construction to the site studied here, but situated outside of the main zone. These sites have further added to the contaminant volume. This material has arisen from the extensive stripping of surface soils, organic material and building demolition to isolate the gamma-emitting radiocesium-containing materials under the present decontamination guidelines published by the Japanese Ministry of the Environment (2013). Such wastes were (and are continuing to be to this date) placed into 1 $m^3$ high-density plastic storage bags which are subsequently sealed and consigned to one of many temporary waste stores that are located across Fukushima Prefecture. It is estimated that tens of thousands of these bags (each weighing several tonnes) will be produced from the proposed clean-up, at a total combined cost of ¥2.53 – ¥5.12 trillion (approximately $22.9 - $46.4 billion as of June 2018) (Yasutaka and Naito, 2016).

The TSSs, such as the site studied herein, are intended to store material on a short-term basis (approximately 3 years – although, in practice this is likely to be much longer). After this time has passed, the long-term solution is to transfer the material from these facilities into a single 'Interim Storage Facility'. This facility is situated in Okuma, nearby to the FDNPP site and has recently begun to accept shipments of waste packages from the numerous TSSs located throughout the prefecture. The sites are often located on the limited flat land across the fallout-affected region – typically the numerous former rice fields that are synonymous with the main crop-type of the Prefecture. After the crop and surface soil is removed from the field the ground is compacted, and the groundworks and drainage networks are installed around and underneath the predetermined location of the waste bags. Within this zone, a geopolymer, specifically engineered to limit seepage of contaminated fluids into the sub-surface, is placed over the ground surface to underly the bags of contaminated material. Only then can the bags of waste be placed onto the site, organised into a body-centred packing arrangement with bags of mountain sand arranged around the exterior of this structure to provide a shielding effect (Japanese Ministry of the Environment, 2013; Shimaoka et al., 2016). Once the bags are arranged as such, the site is capped with a further layer of the polymer material, with drainage and gas ventilation networks installed to exhume gases produced during biodegradation of the contained organic matter (Hardie and McKinley, 2014). Due to the intricate nature of each of these sites, a considerable amount of time is spent not only in preparing the site for the installation of waste bags but also in their careful placement to ensure stability over time. The harsh typhoon environment that is synonymous of this region of Japan – typified by extensive summer and autumn rainfall averaging 1500 mm/year (Japan Meteorological Agency) presents further issues with both construction and long-term care of the site.

In this study, the influence of external effects on the radiological signature of a Fukushima Prefecture waste storage site; *(i)* during the initial construction process and *(ii)* after its completion, are evaluated. Whilst only undertaken at a single test-site, the influence of external factors at other such sites are necessary to ensure the safe temporary storage of this material until it becomes possible to transfer the material to the ISF within Okuma.

## 2. Materials and methods

### 2.1. Survey site

The site selected for analysis during this work was located within the Kawamata Town region of Fukushima Prefecture within the original "Area 2" (latitude/longitude/altitude = 37.593°N/140.701°E/605 m above sea level) close to the neighbouring village of Iitate and the border with "Area 3" – the region most severely contaminated by the accident (Fig. 1). This area was initially contaminated by radiocesium to levels of approximately 4500 kBq $m^{-2}$ (12 μSv $hr^{-1}$) by the accident. At present, the restrictions have been relaxed slightly, and the site is now located outside of the three regions defined as contaminated by the accident (METI, 2017). This area has seen extensive decontamination over recent years and residents once displaced are now permitted to return to their homes. Resulting from the surrounding clean-up and the extensive landscape stripping – this flat site now exists as one of the region's waste stores. As outlined previously, to prepare this site, a flat portion of land was initially stripped of material and overlain with a thickness of sand on an impermeable plastic-based geopolymer material.

During a field study in mid-October 2016 (Connor et al., 2018), the required groundworks prior to installing volumes of the contaminated material on the site had been completed, with the task of carefully positioning the hundreds of waste bags still in-progress. A second visit to the site eight months later during mid-June 2017, was conducted when the site had reached completion – with all material emplaced and "capping" completed.

### 2.2. Unmanned aerial vehicle (UAV)

The aerial system used in this work was constructed at the University of Bristol, UK – with a schematic of the platform and associated detection payload (described below) shown in Fig. 2. The unmanned aerial vehicle (UAV) consisted of an X4 configuration with four electric motors, mounted above four carbon-fibre arms arranged in a cross-arrangement. Using four 30 cm ABS plastic propellers, the UAV had a diameter of 75 cm and a height of 35 cm (when fully assembled). Powered by a single lithium-polymer (LiPo) battery, the UAV was capable of flight times of 15–20 min on a single charge. Without the radiation mapping payload attached, the UAV had a total mass of 3 kg – but with the under-mounted detection system attached, the UAV had a total mass of 5 kg.

Aside from both take-off and landing, which were performed manually using conventional handheld remote controls, the survey flights of the UAV in both instances were undertaken fully-autonomously by creating a pre-determined flight path and uploading this to the UAV via an autopilot software (Mission Planner). At a constant flight velocity of 1.5 $ms^{-1}$ and altitude of 5 m (determined by a combination of the on-board GPS and barometer), the flightpath of the survey consisted of 32 predefined waypoints and took approximately 11 min to complete.

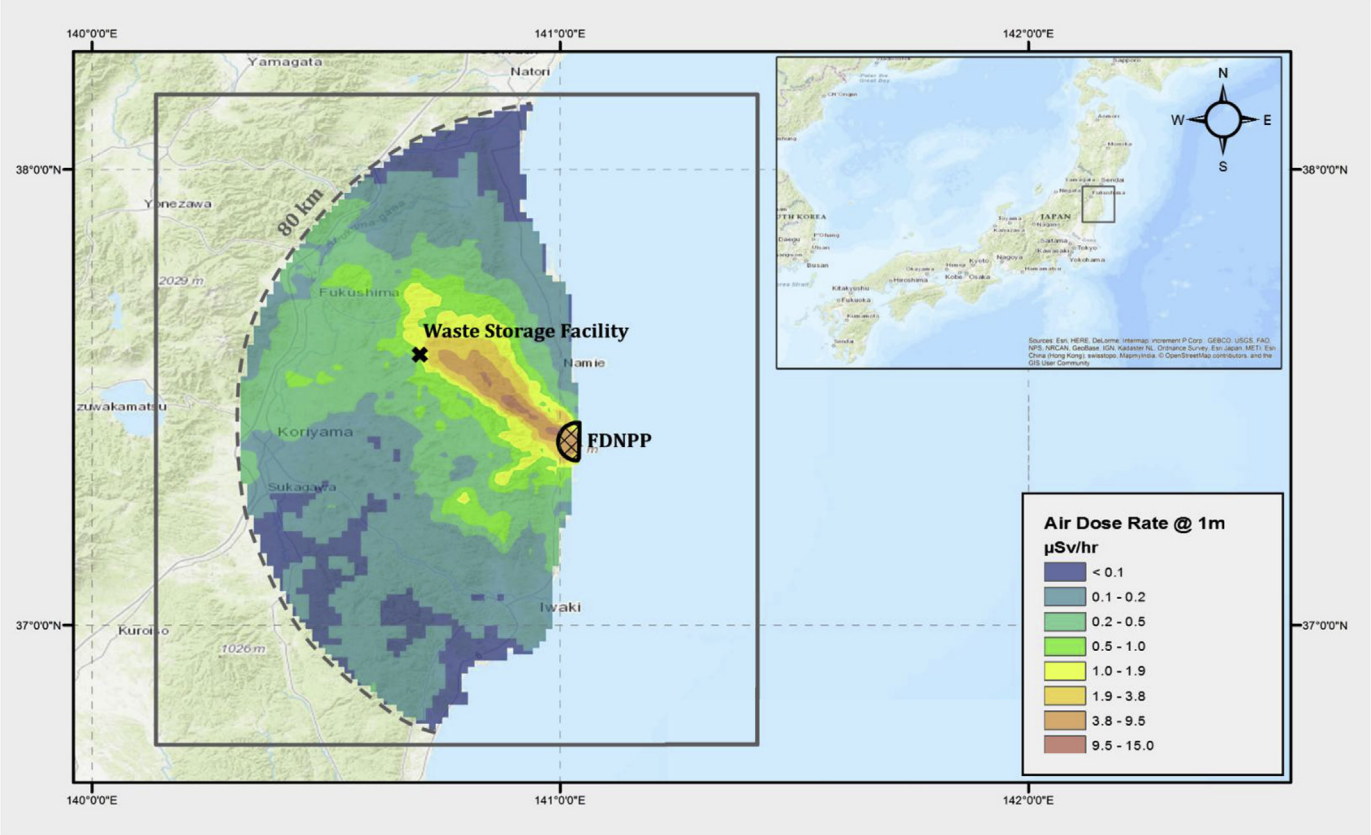


**Fig. 1.** Location of the storage site studied within these works, plotted alongside the distribution of radiological contamination released during the 2011 FDNPP accident.

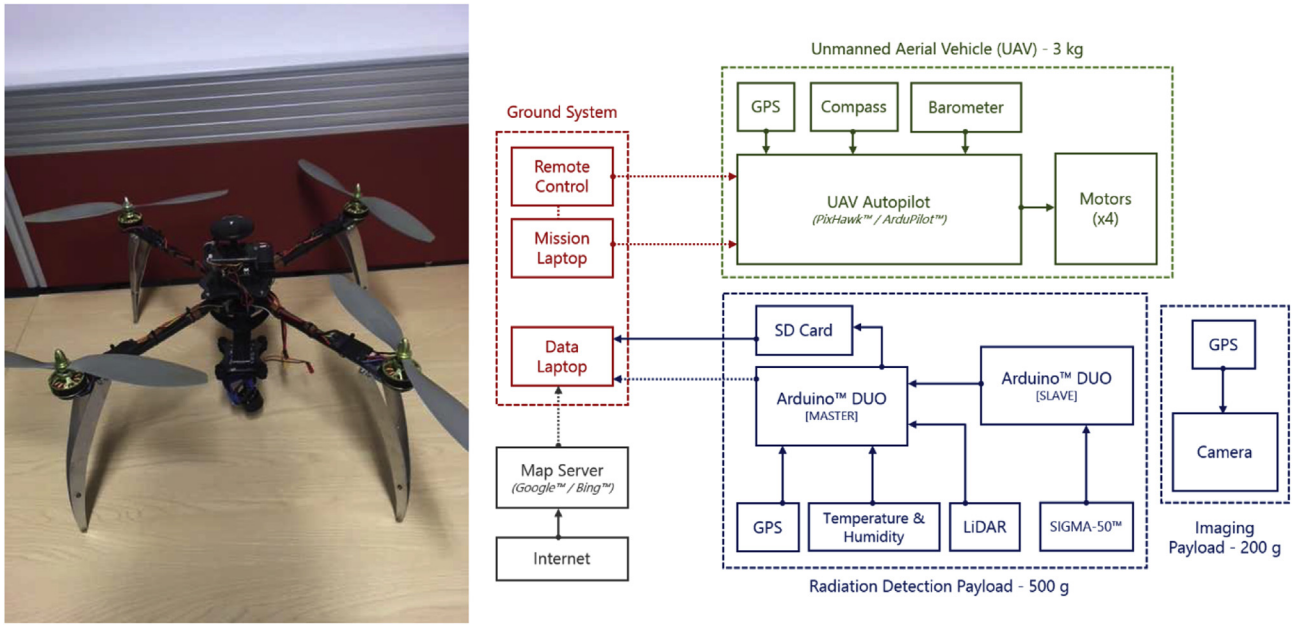


**Fig. 2.** Image and schematic of the UAV and associated detection payloads (radiological and imaging). Solid lines represent the wired connections between devices, with dashed lines the wireless inking of systems. Modified from [1].

[1] P.G. Martin, J. Moore, J.S. Fardoulis, O.D. Payton, T.B. Scott, Radiological Assessment on Interest Areas on the Sellafield Nuclear Site via Unmanned Aerial Vehicle, Remote Sens. 8 (2016c) 913. https://doi.org/10.3390/rs8110913.

### 2.3. Radiation detection & mapping

As mentioned previously, and shown in Fig. 2, the detection payload of the system was mounted beneath the aerial platform between its carbon-fibre legs. Deriving power from the UAV, the radiation detection payload contained its own dedicated GPS unit also mounted on the UAV. Based on the detection system previously described in other works by the authors (MacFarlane et al., 2014; Martin et al., 2015; Martin et al., 2016a; Martin et al., 2016b; Connor et al., 2018), the system used in this work was supplied by ImiTec Ltd. (UK).

The system consisted of a single-point laser rangefinder and radiation detector, contained within an environmentally-sealed plastic enclosure alongside the platform's control electronics. As opposed to earlier works by the authors, a larger volume SIGMA-50 CsI scintillator spectrometer (active volume of 32.8 $cm^3$) is preferred over the smaller volume GR1 CZT semiconductor variant (active volume of 1 $cm^3$)(both from Kromek Ltd. Co. Durham, UK). The premise for the alteration in set-up reflects the overall reduction in measurable radiation intensity within the Fukushima Prefecture through time. Despite the improved energy resolution of the GR1 versus the SIGMA-50 (FWHM of 2.0–2.5% and <7% @ 662 keV respectively), the absolute counts recorded by the detector in the operating environment are too few to present distinct variation in a radiation mapping capacity. An Adafruit™ GPS receiver (position accuracy of approximately 1.8 m (Adafruit Industries, 2016) connected externally to the sealed unit, is placed on the UAV to record the position of the integrated system with every data acquisition. The placement of the receiver is important, for the most accurate position results, it needs to be placed on the main body of the UAV directly above the encased unit. However, to ensure there is no interference, there must be a distinct separation between the GPS receiver for the unit and the UAV. In this configuration, the Adafruit™ GPS unit for the radiation mapping package was placed on the rear arm of the UAV, approximately 60 cm away from the GPS receiver for the UAV. The mapping system (Fig. 2) simultaneously records and stores all of the individual data streams at 10 Hz, these readings are then integrated over 1 s intervals during post-processing.

The laser rangefinder was used to determine the height of the unit above the ground surface to perform a normalisation resulting from the inverse square law of radiation intensity reduction from a point-type source geometry, as described in the method presented in earlier works (Martin et al., 2016a, 2015). During the survey, the UAV was programmed to operate at an altitude of 5 m above ground level (AGL). This survey height was chosen as it was the lowest possible operating altitude that could be achieved whilst still avoiding obstacles within the site.

Before conducting the site survey, the three-dimensional angular response of the detector was analysed within a laboratory setting with a range of radioactive sources (Fig.S1). This experiment indicates that the detection unit is more sensitive to incident gamma rays when placed with its long axis parallel to the ground (Connor et al., 2018). Following the collection, the post-processing of the raw radiation data comprised of removing poorly triangulated recordings (in this instance, this refers to any data points that have recorded communications with less than six satellites), normalising the intensity through the inverse square approximation and integrating the data over 1 s time intervals. The processed data was subsequently converted from raw counts per second (cps) to dose-rate ($\mu Sv\ hr^{-1}$) using the same laboratory-derived calibration described within Connor et al. (2018) (Fig.S2). The resultant dose-rate dataset was then imported as a point shapefile into ArcGIS and interpolated to produce a continuous, colour-scaled dose-rate surface. The resultant layer was subsequently overlain onto the 3D surface model.

## 3. Results & discussion

### 3.1. Aerial photogrammetry

To rapidly produce a three-dimensional rendering of the site as part of this work, aerial photogrammetry was used utilising the same UAV platform used to collect the radiation measurements, albeit with a camera installed in the place of the radiation mapping payload. Once the radiation mapping survey had been completed, a subsequent higher-altitude flight was performed at 25 m. This flight was undertaken at a greater velocity of 3 $ms^{-1}$ with an increased grid separation to ensure sufficient onlap and overlap between the images taken using a GoPro™ Hero5 Black action camera at intervals of one per second. Approximately 235 images were acquired during these flights which were post-processed to generate the detailed topographic site model (Fig. 3). These reconstructions were produced using Agisoft™ Photoscan software, with a full description of the method included within Connor et al. (2018). This mostly autonomous process uses the overlapping regions between each of the two-dimensional aerial images to extract a three-dimensional point cloud of the site. A mesh is then interpolated between these extracted points and coloured using information derived directly from the original images to produce a 3D model. This 3D model is then converted into a digital elevation model (DEM) and a textural overlay (from the initial photos) and imported into ArcGIS to overlay the radiation data. The product DEM created from this process exhibits a spatial resolution of 1.58 cm $pixel^{-1}$ with an RMS reprojection error of 1.56 pixels.

### 3.2. Contaminant distribution

Through processing the aerial radiation survey results of the storage site from the two time-resolved surveys, overlaying radiation data onto the 3-dimensional photogrammetry reconstruction yields the results shown within Fig. 4. The results overlain onto the model of the site from October 2016 are depicted in Fig. 4 (a), with the corresponding model and results from June 2017 shown in Fig. 4 (b). From these results, the clear difference in both the level and extent of the radiological contamination is apparent. Within the model of the site produced following the works of October 2016 (Fig. 4 (a)), a clear plume of heightened activity is observed to extend out to the south of the site. This contamination is believed to result from water (as precipitation) entering, flowing through and then exiting out of the site throughout its construction - when it is yet to be fully covered by its impermeable capping layer (Connor et al., 2018). Despite considerable care being taken to protect against residual contamination of the site during its construction, some migration, however, is highly-likely to occur due to rainwater transiting through the site.

In contrast, the results obtained eight months later illustrate a vastly different contamination regime across the site. As a consequence of the earlier October 2016 survey results having been reported to the site management company, a subsequent phase of clean-up was instigated – with the plume area of contaminated ground extending from the site of the wastes to the south being successfully remediated. To undertake this, the sand material was removed and sent itself for disposal, the source of the leak located and fixed, then replaced with a volume of newly-imported material.

The level of radioactivity exhibited by the large 1 $m^3$ black bags that constitute the bulk of the site is seen to have reduced markedly between the two surveys. In addition to the contribution of radioactive decay – which would have reduced the activity of the material by approximately 4.3% (assuming contributions only from $^{134}Cs$ and $^{137}Cs$), several other factors likely exist to reduce the

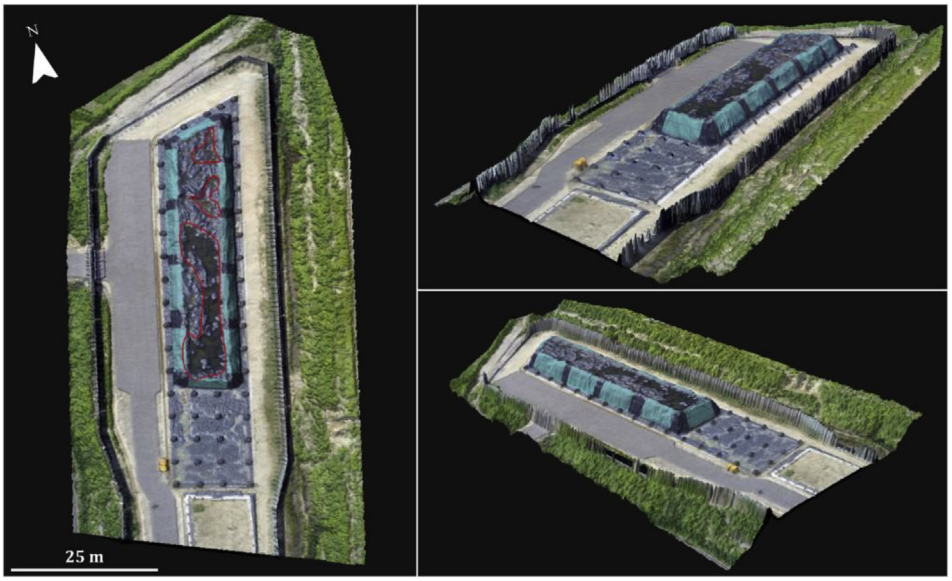


**Fig. 3.** 3-dimensional rendering of the site created from the aerial photographs taken by the UAV. The regions outlined in red indicate water pooling on top of the cover of the waste packages. (For interpretation of the references to colour in this figure legend, the reader is referred to the Web version of this article.)

inherent activity exhibited by the site. One such factor is the covering of the waste bags with the thick (5 mm) impermeable polymer since the completion of the site – a stage that had not been reached in October 2016.

A further factor, apparent from the aerial photogrammetry model shown in Fig. 3, is the volume of rainwater that has pooled onto the top of the waste bags due again to the installation of the highly-impermeable polymer atop the waste material. Being a well-known attenuator of radiation due to its considerable mass-attenuation co-efficient (Hubbell, 1969; NIST, n.d), the varying thickness (measured to be between 20 and 30 cm) of water is more than sufficient to reduce the count-rate by up to approximately 83%–93% over these portions of the site (NIST, n.d).

### 3.3. Contaminant variation

To mathematically evaluate the difference in contamination levels across the site between the two surveys, a plot detailing the mathematic subtraction of the June 2017 results from the October 2016 results is shown within Fig. 5. The plot, created within ArcGIS™, subtracts the CPS values of the cells from the June 2017 dataset (which was first decay-corrected to the date on which the October 2016 dataset was obtained) from the CPS values of the corresponding cells within the October 2016 dataset. The resulting value describes whether radiation intensity has increased, or decreased, within the cell as a collective product of the factors discussed earlier.

Resulting from this process, the mean site-wide reduction in measured intensity is calculated to be 7.1%. However, as can be identified from Fig. 5, there are regions which have experienced more significant levels of change than this mean value. This variation manifests as localised reductions and increases in the measured intensity relative to the October 2016 values in different areas of the site. The largest reduction (60–82%) is measured around the south-western edge of the bale stack and represents the successful remediation of the aforementioned southward extending plume. The largest increase (40–46%), however, is measured within the north-eastern corner of the site and is linked to the broad hotspot that is evident within the June 2017 survey, but absent within the October 2016 survey.

Whilst this may be a true reflection of the contaminant distribution in this zone, it may also be possible that the airborne detector system is measuring increased intensity contributions from outside the remediated zone (fenced area) relative to the ground-based unit used within the 2016 investigation. This characteristic is termed an 'edge effect' and has likely had the effect of erroneously increasing the measured intensity. If this is indeed the mechanism that is occurring, then its effect would be most pronounced in the acute (north-eastern) corner of the site, where the rising bank to the former paddy field above begins to wrap around this corner. Considering the source to detector geometry, there is much higher proportion of 'unremediated' ground that could be sampled by the detector in this corner when compared against the rest of the site. Around the rest of the perimeter, the paddy fields step down in elevation, meaning that any less well remediated land (i.e. the banks) are in a geometrically unfavourable configuration to influence the survey in this way. Hence, this effect is observed proximal to the step-up boundary along the eastern and north eastern perimeters of the site.

Focussing specifically on the bale region of the site, the impermeable cover that has been placed over the bale stack has reduced the measured intensity emitted from this region by an average of 14.1%. As previously mentioned, the water that can be seen pooling on top of the bale stack is also likely to have an attenuating effect upon the emitted intensity. This effect is exhibited within the results of this survey. By isolating the areas that can be seen to have water present within the orthophoto of the site, the average reduction in measured intensity in these regions is calculated to be 21.0%.

### 3.4. Spectrometry analysis

The gamma-ray spectra attained at two points on the site after the June 2017 radiation survey are presented in Fig. 6(a) and (b). Each spectrum was recorded over 20 mins using the same detector placed directly onto the target surface. What is immediately apparent from these spectral results are the differing peaks and, therefore contributing species, in each of these locations.

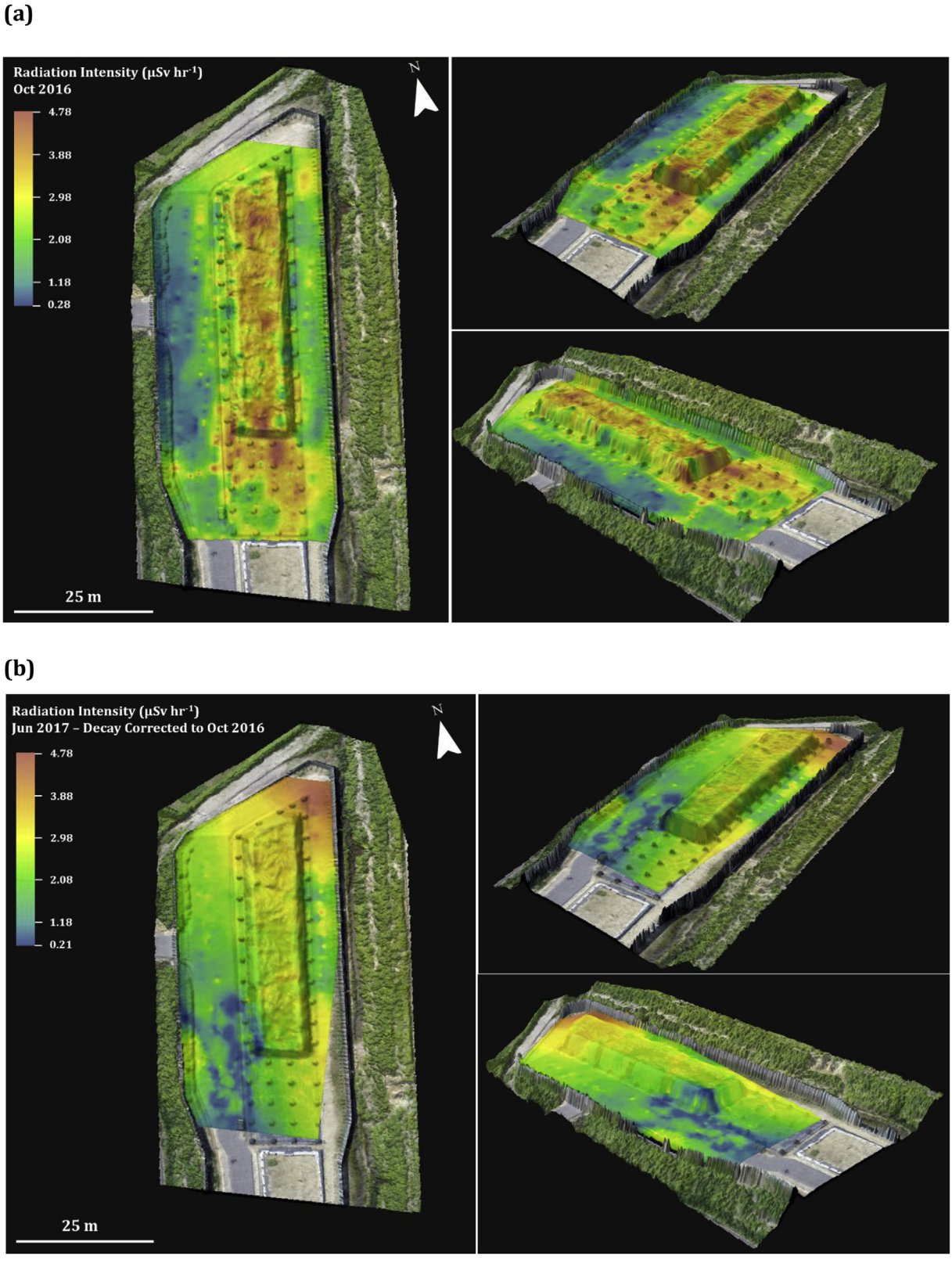


**Fig. 4.** 3-dimensional radiation overlay maps constructed from data recorded at the waste storage site during; (a) October 2016 and (b) June 2017.

Corresponding to the waste material bags at the centre of the site (dose rate of 3.59 μSv $hr^{-1}$), as expected, the radionuclide peaks present are those of the principal contaminant species, Cs – namely the longer-lived $^{137}$Cs (half-life = 30.05 years), but also to a lesser extent the much shorted-lived $^{134}$Cs (half-life = 2.065 years). However, given that the initial activity ratio of $^{134}$Cs:$^{137}$Cs released during the accident was 1:1, much of this shorter-lived isotope has now decayed into the stable barium isotope $^{134}$Ba. The spectrum,

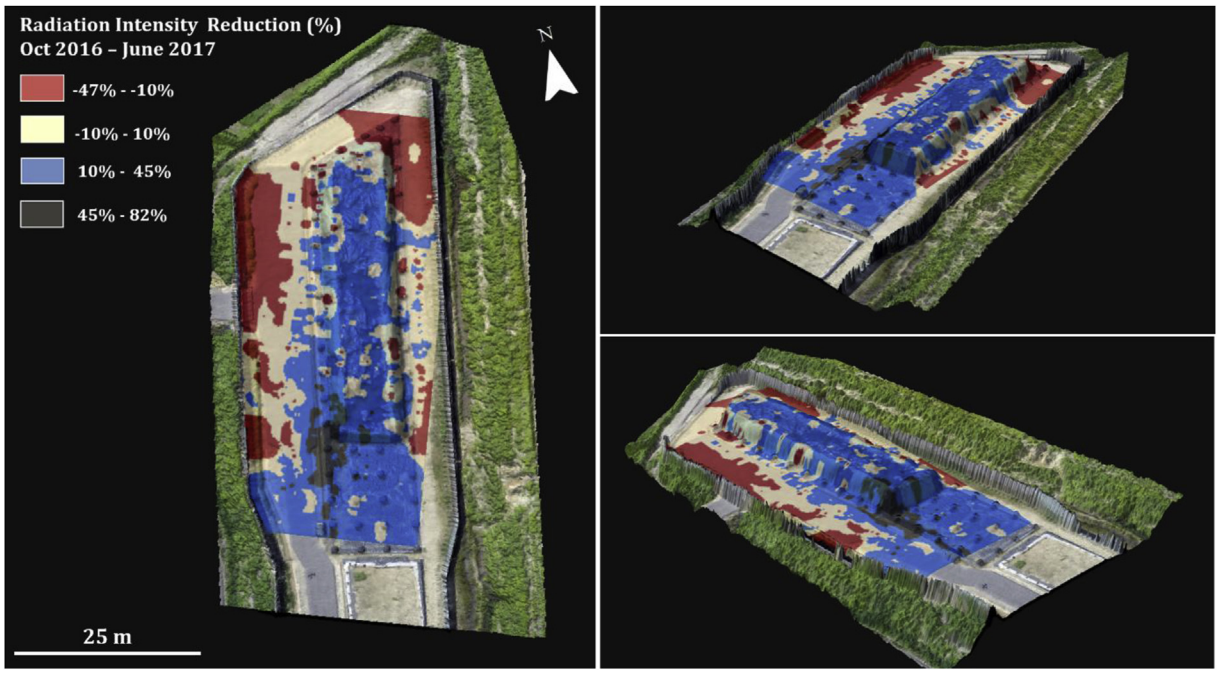


**Fig. 5.** Radiation contamination intensity plot, detailing the change in radioactivity at each georeferenced position across the site between the two surveys (9 months) in October 2016 and June 2017.

recorded with the detector resting on the covering geopolymer, is shown in Fig. 6 (a). In contrast to this is the spectrum acquired over region away from these storage bags that has since been overlain by sand, with the characteristic portion shown in Fig. 6 (b). Whilst this area shows considerably less radioactivity (dose rate of 0.62 μSv $hr^{-1}$) than the area at the other end of the site where the vast quantity of waste bags is located – a gamma signature is nonetheless obtained with the detector in direct contact with the ground.

This window of the spectrum does not contain contributions from the radioisotopes of Cs, suggesting the remediation has been exceptionally effective. Instead, apparent within the spectra are the gamma-ray peaks associated with the decay of the uranium decay-chain members $^{226}$Ra (186 keV), $^{214}$Bi (609 keV) and $^{214}$Pb (240 and 351 keV).

### 3.5. Integrating UAVs within large-scale mapping procedures

Due to the large volume of contaminated material being generated by the remediation processes, there are now a vast number of TSSs throughout the Fukushima Prefecture, with more being created as new land becomes available - either through increased land stripping or regions becoming more accessible as the overall radiation intensity reduces through time. Monitoring these sites is a hugely labour-intensive process, involving numerous ground-based surveys repeated throughout defined time intervals. Whilst this method produces high-resolution results, there are a few issues that could be improved upon.

Firstly, human operators can attenuate as much as 35% of the incoming radiation that would otherwise be incident upon the detector (Buchanan et al., 2016; Connor et al., 2016). As this effect is non-standard for different body shapes and sizes, this reduces comparability of the results between surveys conducted by different operators. Furthermore, human operators are inherently poor at repeating the same survey and walking in consistently spaced parallel lines, which further reduces comparability. Conversely, UAV systems experience no operator-related attenuation effects and can be programmed to follow a predefined flight path with a good-degree of accuracy. This not only improves map-to-map comparability versus a human carrier, but also translates to a radiation dose saving for the operator, who would otherwise have to manually move the detector system around the environment.

There is also the potential for a time saving component through utilising UAVs within these surveys. As target sites become increasingly large or topographically variable, the time taken for a human operator to effectively cover the area increases significantly. As UAVs are terrain independent, the time taken to survey these areas increases less significantly with increasing area or topographic complexity, representing a greater temporal efficiency for UAV surveys versus ground-based surveys. It must be noted however, that to maintain safe operations, the UAV systems require an initial set-up and safety check period, hence for small and simple sites, UAV operations may take longer to conduct than the equivalent ground-based survey.

In order to assess the potential time-saving nature of UAV-hosted radiometric surveying for this site a comparative ground-based survey was conducted alongside the airborne radiometric survey and assessed for the time taken to complete the survey. In order to be fully comparable, the human operator attempted to mimic some chosen parameters of the UAV survey, including the survey line spacing (approximately 1.5 m) and the bounding perimeter. Considering the total survey time for each method, including the safety assessment and flight planning stages of the UAV survey, the ground-based survey took 58 min to complete, whereas the entire UAV survey process was completed in 44 min; saving 14 min in a single survey. Whilst the site in question is not particularly large (approximately 3900 $m^2$), for the ground-based survey to achieve a similar coverage to the UAV survey, the operator had to physically walk over the bale stack, which slowed down the progress of the survey. Given that every TSS follows a similar basic structure, all the sites will contain a similar difficult terrain for human operators to cover. As a UAV survey managed to save 15 min

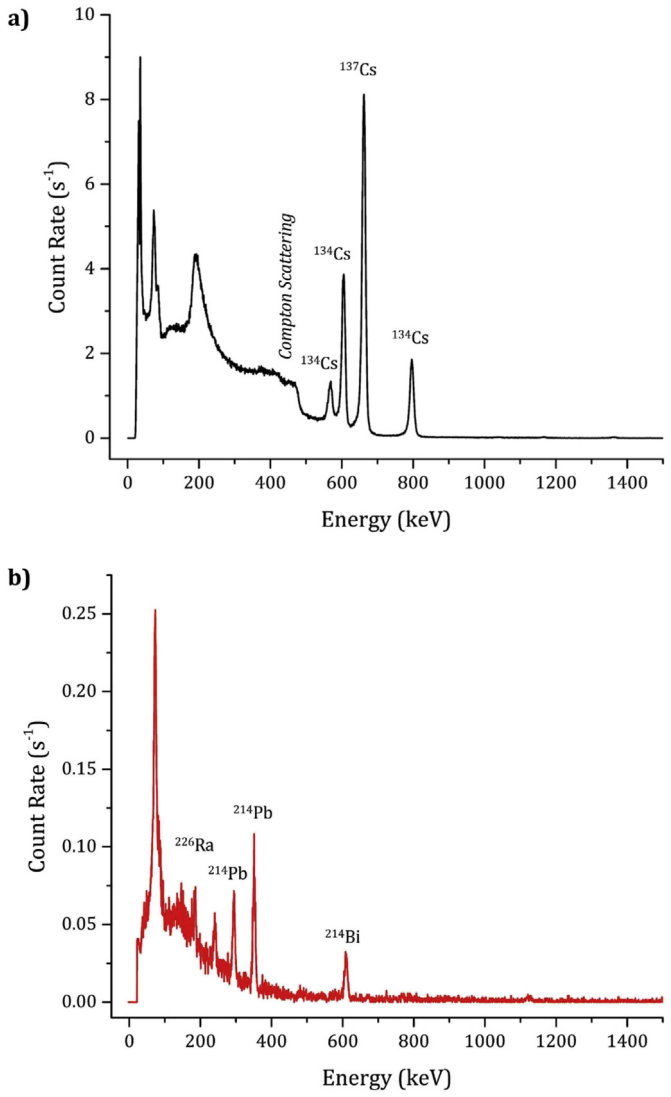


**Fig. 6.** Gamma-ray spectra subsequently obtained at different positions at the survey site, using the same SIGMA-50 detector used for during surveys. The spectra shown were collected at; (a) on-top of the contaminant wastes, and (b) on the sand imported to cover the storage site.

within a single site survey, this could potentially represent a significant time saving method of monitoring these TSSs, as well as significantly reducing the potential dose for the operator.

Airborne radiation mapping is already a prominent technique utilised with the response and remediation work that is ongoing within Japan. These surveys, carried out regularly by MEXT and the Japanese government, utilise large fixed-wing aircraft and much larger volume NaI detectors than can be used on a UAV. This configuration of airborne radiation mapping systems is highly advantageous for covering large areas rapidly, but comes at a loss of spatial resolution (Connor et al., 2016; Pitkin and Duval, 1980; Sanada and Torii, 2014). The larger, manned aircraft (fixed-wing aeroplanes and helicopters) cannot fly at lower altitudes for regulation and safety reasons, limiting them to an operational altitude of between approximately 90 m–250 m (figures obtained from Beamish, 2014 and Pitkin and Duval, 1980 respectively), although surveys seem to aim for approximately 90–120 m altitude wherever possible. For a stationary detector at 90 m altitude, 90% of the radiation detected will be emitted from a circle of approximately 240 m radius, whereas a detector operating at 10 m samples the much smaller radius of 60 m (Pitkin and Duval, 1980). In a practical sense, this data pertains to the use of larger volume detectors than used within this study, hence, the ground sampling radius of the lower volume detectors is likely to be much smaller than can be predicted using this model. As a result of the smaller ground sampling radius and a lower operating altitude (in this study 5 m), the UAV radiation mapping systems are better suited to monitoring smaller sites, such as those presented by the thousands of TSSs around the Fukushima Prefecture.

Whilst UAV operations may represent significant savings in both radiation dose and time, this does not mean that these methods are superior to other ground-based systems in every case. The platform used within any survey must be appropriate to achieve the intended outcomes of the investigation. For example, if a survey aimed to assess the dose received by a member of the public as they approached a TSS, such as the one studied herein, then a ground-based system would likely prove more appropriate than an aerial platform, as this best simulates the path that a human would take towards a site. Furthermore, multi-rotor UAV platforms are still weight-limited in what they can carry as a payload. In practice, this limits the radiation mapping systems to using small volume detectors, which are not as well suited to collecting spectral information. This is due to a number of reasons, which are outlined in extensive detail in Gilmore (2008) and Knoll, 2010. Despite this, when used appropriately, the methods that utilise UAVs over ground-based systems can show significant improvements in several important metrics.

## 4. Conclusions & future work

This work has provided several key findings relevant to both the low altitude remote sensing of contaminated environments as well as the work that has been performed specifically at this site. Via an unmanned aerial vehicle, it has been possible to provide a time-resolved visualisation of contamination across a site – showing the positive influence of the remediation that occurred. Over the eight-month period between the two surveys, the radioactivity levels detected from the wastes located at the centre of the site had decreased – representing the combination of several factors, including natural radioactive decay, as well as surface covering by both an impermeable capping layer and a varying depth of water.

The overall success of this clean-up operation can be attributed to the ongoing collaboration between the authors and the Japanese authorities tasked with the monitoring of these sites. The open-channel communication between the two parties has been proven to be effective in evaluating whether contaminated material has been contained within the packaging exposed during the construction period of a TSS and in highlighting areas in which remediation efforts should be focussed. Following the data collection, the analysis of the results from the initial survey was communicated back to the regional managing authority, who used the maps created from the survey to implement a bespoke strategy to alter areas for concern; such as the southwards extending plume shown within the results from October 2016.

Future work will assess the repeatability of the UAV radiometric surveys through the implementation of repeat surveys within a number of temporary storage facilities. This investigation will primarily focus on comparing the radiation maps produced from flying the same flightpaths over a series of days but will also assess the speed of deployment and flight-line deviation throughout the survey. Once complete, this investigation will determine the suitability of a regional scale UAV radiometric survey programme for continual site assessment not only within the test area of Japan, but potentially for many radiological sites worldwide.

## Acknowledgements

The authors wish to thank the Daiwa Anglo-Japanese Foundation (Ref: 6102/12029) for kindly providing funding to enable the October 2016 fieldwork within Japan. Support from local officials and members of the public within Fukushima Prefecture is greatly appreciated for facilitating access to such study sites.

D. Connor acknowledges funding from both the EPSRC (EP/N509619/1) and National Nuclear Laboratory's Characterisation IR&D Programme (NNL/UA/037). P. Martin would like to thank alumni Elaine and Perry Noble for their support through the DJ Noble Scholarship. N. Smith is funded by a Royal Society Industry Fellowship and acknowledges funding from the National Nuclear Laboratory's Characterisation IR&D Programme. Finally, the authors would also like to thank the four reviewers for their time and expertise during the review process, their constructive and detailed comments have added invaluable contributions to the manuscript.

## Appendix A. Supplementary data

Supplementary data related to this article can be found at https://doi.org/10.1016/j.envpol.2018.08.099.

## References

Adafruit Industries, 2016. Adafruit Ultimate GPS 1–29.

Aoyama, M., Hamajima, Y., Hult, M., Uematsu, M., Oka, E., Tsumune, D., Kumamoto, Y., 2016. 134Cs and 137Cs in the north Pacific ocean derived from the March 2011 TEPCO Fukushima Dai-ichi nuclear power plant accident, Japan. Part one: surface pathway and vertical distributions. J. Oceanogr. 72, 53–65. https://doi.org/10.1007/s10872-015-0335-z.

Beamish, D., 2014. Environmental radioactivity in the UK: the airborne geophysical view of dose rate estimates. J. Environ. Radioact. 138, 249–263. https://doi.org/10.1016/j.jenvrad.2014.08.025.

Buchanan, E., Cresswell, A.J., Seitz, B., Sanderson, D.C.W., 2016. Operator related attenuation effects in radiometric surveys. Radiat. Meas. 86, 24–31. https://doi.org/10.1016/j.radmeas.2015.12.029.

Buesseler, K., Dai, M., Aoyama, M., Benitez-Nelson, C., Charmasson, S., Higley, K., Maderich, V., Masqué, P., Morris, P.J., Oughton, D., Smith, J.N., 2017. Fukushima Daiichi–derived radionuclides in the ocean: transport, fate, and impacts. Ann. Rev. Mar. Sci. 9, 173–203. https://doi.org/10.1146/annurev-marine-010816-060733.

Comans, R.N.J., Hockley, D.E., 1992. Kinetics of cesium sorption on illite. Geochem. Cosmochim. Acta 56, 1157–1164. https://doi.org/10.1016/0016-7037(92)90053-L.

Connor, D., Martin, P.G., Scott, T.B., 2016. Airborne radiation mapping: overview and application of current and future aerial systems. Int. J. Rem. Sens. 37, 5953–5987. https://doi.org/10.1080/01431161.2016.1252474.

Connor, D.T., Martin, P.G., Smith, N.T., Payne, L., Hutton, C., Payton, O.D., Yamashiki, Y., Scott, T.B., 2018. Application of airborne photogrammetry for the visualisation and assessment of contamination migration arising from a Fukushima waste storage facility. Environ. Pollut. 234, 610–619. https://doi.org/10.1016/j.envpol.2017.10.098.

Cremers, A., Elsen, A., Preter, P. De, Maes, A., 1988. Quantitative analysis of radiocaesium retention in soils. Nature 335, 247–249. https://doi.org/10.1038/335247a0.

Gilmore, G.R., 2008. Practical Gamma-Ray Spectrometry. John Wiley & Sons, Ltd, Chichester, UK. https://doi.org/10.1002/9780470861981.

Hardie, S.M.L., McKinley, I.G., 2014. Fukushima remediation: status and overview of future plans. J. Environ. Radioact. 133, 75–85. https://doi.org/10.1016/J.JENVRAD.2013.08.002.

Hubbell, J.H., 1969. Photon cross sections, attenuation coefficients and energy absorption coefficients from 10 keV to 100 GeV. Natl. Stand. Ref. Data Ser.

Japan Meteorological Agency, n.d. Monthly Total of Precipitation (Mm) - Japan Meteorological Agency ([WWW Document]).

Japanese Ministry of the Environment, 2013. Decontamination Guidelines, second ed.

Knoll, G.F., 2010. Radiation Detection and Measurement. John Wiley & Sons.

Kurokawa, K., Ishibashi, K., Oshima, K., Sakiyama, H., Sakurai, M., Tanaka, K., Tanaka, M., Nomura, S., Hachisuka, R., Yokoyama, Y., 2012. The National Diet of Japan: Fukushima Nuclear Accident Independent Investigation Commission. Natl. Diet Japan.

MacFarlane, J.W., Payton, O.D., Keatley, a. C., Scott, G.P.T., Pullin, H., Crane, R. a., Smilion, M., Popescu, I., Curlea, V., Scott, T.B., 2014. Lightweight aerial vehicles for monitoring, assessment and mapping of radiation anomalies. J. Environ. Radioact. 136, 127–130. https://doi.org/10.1016/j.jenvrad.2014.05.008.

Martin, P.G., Payton, O.D., Fardoulis, J.S., Richards, D.A., Scott, T.B., 2015. The use of unmanned aerial systems for the mapping of legacy uranium mines. J. Environ. Radioact. 143, 135–140. https://doi.org/10.1016/j.jenvrad.2015.02.004.

Martin, P.G., Kwong, S., Smith, N.T., Yamashiki, Y., Payton, O.D., Russell-Pavier, F.S., Fardoulis, J.S., Richards, D.A., Scott, T.B., 2016a. 3D unmanned aerial vehicle radiation mapping for assessing contaminant distribution and mobility. Int. J. Appl. Earth Obs. Geoinf. 52, 12–19. https://doi.org/10.1016/j.jag.2016.05.007.

Martin, P.G., Payton, O.D., Fardoulis, J.S., Richards, D.A., Yamashiki, Y., Scott, T.B., 2016b. Low altitude unmanned aerial vehicle for characterising remediation effectiveness following the FDNPP accident. J. Environ. Radioact. 151, 58–63. https://doi.org/10.1016/j.jenvrad.2015.09.007.

METI, 2011. Restricted Area, Deliberate Evacuation Area and Regions Including Specific Spots Recommended for Evacuation ([WWW Document]).

METI, 2015. Areas to Which Evacuation Orders Have Been Issued ([WWW Document]).

METI, 2017. Six years later: Fukushima now, steadily making progress toward a brighter future. METI J 4–13.

NIST, n.d. X-Ray Mass Attenuation Coefficients - Water, Liquid [WWW Document]. URL https://physics.nist.gov/PhysRefData/XrayMassCoef/ComTab/water.html (accessed 4.10.18).

Pitkin, J.A., Duval, J.S., 1980. Design parameters for aerial gamma-ray surveys. Geophysics 45.

Sanada, Y., Torii, T., 2014. Aerial radiation monitoring around the Fukushima Dai-ichi nuclear power plant using an unmanned helicopter. J. Environ. Radioact. 139, 294–299. https://doi.org/10.1016/j.jenvrad.2014.06.027.

Sawhiney, B., 1972. Selective sorption and fixation of cations by clay minerals: a review. Clay Clay Miner.

Shimaoka, T., Kumagai, K., Katsumi, T., Iba, M., 2016. Design, installation, and maintenance of temporary storage sites for radioactive decontamination waste. Japanese Geotech. Soc. Spec. Publ. 2, 2385–2390. https://doi.org/10.3208/jgssp.IGS-44.

Steinhauser, G., Brandl, A., Johnson, T.E., 2014. Comparison of the Chernobyl and Fukushima nuclear accidents: a review of the environmental impacts. Sci. Total Environ. 470–471, 800–817. https://doi.org/10.1016/J.SCITOTENV.2013.10.029.

Yasutaka, T., Naito, W., 2016. Assessing cost and effectiveness of radiation decontamination in Fukushima Prefecture, Japan. J. Environ. Radioact. 151, 512–520. https://doi.org/10.1016/j.jenvrad.2015.05.012.